PCCP

Accepted Manuscript

ROYAL SOCIETY OF CHEMISTRY

www.rsc.org/pccp

Ag nanoparticles-anchored reduced graphene oxide catalyst for oxygen electrode reaction in aqueous electrolytes and also a non-aqueous electrolyte for Li-O_2 cells

Surender Kumar[a], C. Selvaraj[a], L. G. Scanlon[b] and N. Munichandraiah*[a]

[a]Department of Inorganic and Physical Chemistry, Indian Institute of Science – 560012

[b]Air Force Research Laboratory, Electrical Systems Branch, Wright-Patterson Air Force Base, Ohio 45433, USA

*Email: muni@ipc.iisc.ernet.in (corresponding author)

Abstract:

Silver nanoparticles-anchored reduced graphene oxide (Ag-RGO) is prepared by simultaneous reduction of graphene oxide and Ag^+ ions in an aqueous medium by ethylene glycol as the reducing agent. Ag particles of average size of 4.7 nm are uniformly distributed on the RGO sheets. Oxygen reduction reaction (ORR) is studied on Ag-RGO catalyst in both aqueous and non-aqueous electrolytes by using cyclic voltammetry and rotating disk electrode techniques. As the interest in non-aqueous electrolyte is to study the catalytic performance of Ag-RGO for rechargeable Li-O_2 cells, these cells are assembled and characterized. Li-O_2 cells with Ag-RGO as the oxygen electrode catalyst are subjected to charge-discharge cycling at several current densities. A discharge capacity of 11,950 mAh g^{-1} (11.29 mAh cm^{-2}) is obtained initially at low a current density. Although there is a decrease in capacity on repeated discharge-charge cycling initially, a stable capacity is observed for about 30 cycles. The results indicate that Ag-RGO is a suitable catalyst for rechargeable Li-O_2 cells.

Introduction

Oxygen reduction reaction (ORR) is one of the most important reactions studied extensively in electrochemical energy storage applications.[1] In proton-exchange membrane fuel cells employing H_2 or methanol as the fuel undergoing electrooxidation at the anode, O_2 supplied to the cathode undergoes reduction.[2] In metal-air batteries, such as Zn-air system, O_2 present in the atmosphere undergoes reduction at the cathode in an aqueous electrolyte.[3] As the atmosphere is a rich source of O_2, it is employed free of cost in air-breathing mode in these battery systems. In recent years, there is a surge of interest on ORR in non-aqueous media also for applications such as Li-air batteries.[4]

Research activities on Li-air (or, Li-O_2) battery system have received increasing interest in recent years.[5] This battery has a high theoretical specific energy (11.68 $kWhkg^{-1}$), which is expected to be a clean and environmental friendly alternate energy source to gasoline for vehicular traction.[5] The cell consists of Li metal as the anode and a carbon-based porous oxygen electrode as the cathode in a suitable non-aqueous electrolyte. While the development of primary Li-air system may not involve serious problems, the development of rechargeable battery is tedious with serious problems arising from several sources. Among them, studies on rechargeable O_2 electrode with fast kinetics of ORR during the cell discharge and oxygen evolution reaction (OER) during charge in non-aqueous electrolytes are important. In aqueous electrolytes, ORR occurs in two pathways: the direct 4-electron reduction pathway from O_2 to H_2O and the 2-electron reduction pathway from O_2 to H_2O_2 followed by the formation of H_2O.[6] In non-aqueous electrolytes, the 1-electron reduction of O_2 to superoxide (O_2^-) is known to occur as the first step.[7] This step is followed by the formation of peroxide and oxide.

The kinetics of ORR is slow in both aqueous and non-aqueous electrolytes.[1] Furthermore, the reaction needs to be reversible for application in rechargeable Li-air battery. In order to realize ORR with fast kinetics, a suitable catalyst is essential. Additionally, the catalyst should be

bifunctional for both of ORR and OER in a rechargeable battery. Platinum-based materials are known as the most appropriate catalysts for ORR in aqueous electrolytes. However, Pt is expensive and its resources are limited. It is desirable to explore non-platinum metals, or atleast to reduce the amount of Pt in device applications. For instant, Di Noto et al., studied PtNi and $PtFe_2$ bimetallic systems,[8] PtRu carbon nitrides[9,10] and PdNi bi- as well as PdCoNi tri-metallic[11] systems for studies related to polymer electrolyte membrane fuel cell. Silver is inexpensive and it also has a moderately high catalytic activity towards ORR in aqueous media.[12]

Graphene has two-dimensional planar structure with sp^2 bonded carbon atoms. It has become an important electrode material owing to its high electronic conductivity and large surface area.[13] It has been used as an electrode material for applications such as supercapacitors, Li-ion batteries, and fuel cells.[14-16] Catalyst nanoparticles prepared and anchored to graphene sheets are expected to sustain discrete existence without undergoing agglomeration and therefore they possess a high catalytic activity for prolonged applications. Lim et al.,[17] prepared Ag nanoparticles on reduced graphene oxide (RGO) by simultaneous reduction of Ag^+ ions and graphene oxide (GO) by $NaBH_4$ and electrocatalytic activity was studied for ORR in an alkaline medium. Ag particles of average diameter of 10 nm were distributed on RGO sheets. The Ag-RGO exhibited greater catalytic activity than Ag-C towards ORR in O_2 saturated 0.1 M NaOH electrolyte. Ag-graphene nanoribbons were prepared by chemical unzipping of multiwalled carbon nanotubes with a Ag-salt in the reaction medium.[18] The catalytic activity of this composite towards ORR was greater than a commercial Ag-C catalyst in 0.1 M KOH electrolyte. Ag-RGO hybrid with evenly distributed nanoparticles of Ag on RGO was prepared from an aqueous suspension consisting of graphene and $Ag(NH_3)_2OH$ solution by reduction using hydrazine.[19] The hybrid material was studied for electrochemical actuator design. There are no studies on catalytic activity of Ag-RGO in Li-O_2 cells reported till now.

In the present work, Ag nanoparticles anchored reduced graphene oxide (Ag-RGO) is prepared by in-situ reduction of graphene oxide (GO) and Ag^+ ions by ethylene glycol as the reducing agent. Nearly spherical Ag particles of average size of 4.7 nm are uniformly anchored on graphene sheets. The average particle size of Ag nanoparticles is considerably smaller than the value is reported in the literature.[17] The Ag-RGO is employed as a catalyst for studies of ORR both in aqueous and non-aqueous electrolytes. Li-O_2 cells assembled in a non-aqueous electrolyte using Ag-RGO as the catalyst for bifunctional ORR-OER rechargeable electrode deliver a high discharge capacity with a reasonably good charge-discharge cycling stability. To the best of authors' knowledge catalytic activity of Ag-RGO for rechargeable oxygen electrode in Li-O_2 non-aqueous cells is reported for the first time.

Experimental:

Graphite powder (Graphite India), $NaNO_3$, $KMnO_4$, KOH, ethylene glycol, $AgNO_3$ (all from S. D. Fine Chemicals), $LiPF_6$, polyvinylidene fluoride (PVDF), n-methyl pyrrolidone (NMP), dimethyl sulphoxide (DMSO), tertabutyl ammonium perchlorate (TBAP), lithium ribbon (all from Aldrich) and NaCl (Qualigens) were used as received. Double-distilled water was used for all experiments during the preparation of RGO and Ag-RGO, and for preparation of aqueous solutions.

For the preparation of Ag-RGO, graphite powder was first converted into graphite oxide (GtO) by the procedure described by Hummers and Hoffeman.[20] In brief, graphite powder (3.0 g) was added to 69 ml concentrated H_2SO_4 with 1.50 g $NaNO_3$ dissolved in it. The mixture was stirred for 1h at ambient temperature. The container was cooled in an ice bath and 9.0 g $KMnO_4$ was added slowly while stirring the contents vigorously by a magnetic stirrer for about 15 min. The container was removed from the ice bath and allowed to warm up to ambient temperature. Two aliquots of 138 ml and 420 ml double-distilled water were added slowly and carefully in about 15 min intervals. Subsequently, 7.5 ml 30% H_2O_2 was added and the colour of the suspension changed from light yellow to brown, indicating the oxidation of graphite to GtO. The

product GtO was separated by centrifugation washed with warm water and ethanol several times and dried at 50 ^{0}C for 12 h. GtO (400 mg) was transferred into 800 ml double-distilled water and sonicated for 3 h. GtO was exfoliated to graphene oxide (GO) by sonication, which was separated by centrifugation, washed with double-distilled water and ethanol followed by drying at 50 ^{0}C for 12 h. $AgNO_3$ (157 mg) was added to 100 mg GO was dispersed in 600 ml double-distilled water, sonicated for 30 min, then 1 M KOH (100 ml) was added slowly while stirring the contents. Finally, 1 M ethylene glycol (100 ml) was added as a reducing agent and the container was kept at 80 ^{0}C for 3 h while stirring the contents. The product, Ag-RGO was separated by centrifugation, washed copiously with double-distilled water and ethanol, and dried at 60 ^{0}C for 12 h. The quantities of $AgNO_3$ (157 mg) and GO (100 mg) were taken for the formation of Ag-RGO with mass ratio of Ag:RGO at 1:1. The product Ag-RGO was analyzed for the quantity of Ag by inductively coupled plasma emission spectroscopy and the quantity Ag present in Ag:RGO was 47 wt%, which closely agrees with the theoretical value (50 wt%).[21] RGO was also prepared in a similar procedure in the absence of $AgNO_3$.

For the electrochemical characterization studies by rotating disc electrode (RDE), 1.8 mg Ag-RGO and 4 µl Nafion (5 wt% solution) were dispersed in 2 ml ethanol by sonication for 30 min. The suspension (200 µl) was dropped on a glassy carbon (GC) disk electrode of area 0.07 cm^2 (diameter: 3mm) and solvent was evaporated in air. The quantity of Ag–RGO composite was 200 µg on the GC electrode (2.8 mg cm^{-2}). For the preparation of O_2 electrodes for Li-O_2 cells, porous carbon paper (Toray) of 2.0 mm thickness was used as the current collector. One side of the carbon paper was coated with carbon diffusion layer and the other side with the catalyst layer. A circular (12 mm diameter) disk was punched out of a sheet of Toray carbon paper. High surface area (1500 cm^2 g^{-1}) carbon powder (Fuzhou Yihuan Carbon, Co., China) and PTFE suspension (Aldrich) were mixed in 7:3 weight ratio. A minimum quantity of water was added to form dough, which was rolled into a layer. This layer (13 mg cm^{-2}) was applied on one side of the carbon paper current collector. The Ag-RGO catalyst and PVDF were mixed (weight

ratio: 92.5:7.5) in a mortar, a few drops of NMP were added to form an ink. The ink was coated on the other side of the carbon paper. The mass of catalyst was 1 mg cm^{-2}. The sandwich of diffusion-layer, carbon paper and catalyst-layer was pressed in a die at a pressure of 50 kN for 3 min. The electrode was dried at 100 ^{0}C for 12 h and transferred into an argon filled MBraun glove box model Unilab. Li-O_2 cells were assembled in home-made Swagelok-type PTFE containers. The container had provision to close on one side where Li disk anode was placed and the other side open for exposure to oxygen gas from a cylinder. A Li disk used as the anode (12 mm diameter) was punched out of a ribbon (0.3 mm thick) and its surface was scraped with a knife to remove a surface layer on both sides of it. Stainless steel current collectors were used to take electrical contacts from the electrodes. The Li disk, a glass mat separator and the air electrode were sandwiched inside the PTFE container and stainless steel electric contacts were inserted and sealed.[22-24] The glass mat was soaked in the electrolyte, which was made of 1.0 M $LiPF_6$ in DMSO, before inserting into the cell. The catalyst-layer of the O_2electrode was exposed to the electrolyte and the diffusion-layer to oxygen gas.

For sonication during different stages of preparation of RGO and Ag-RGO, a Misonix ultra sonicator model S4000-010 was used. It was operated with a frequency of 20 kHz and power output of 600W. Titanium horn (diameter = 12 mm) was dipped in the aqueous phase and sonicated for the required duration. A Remiultracentrifuge model R-8C was used to separate the solid samples from liquid phase. Powder X-ray diffraction patterns were recorded using a Philips 'X'PERT PRO diffractometer with Cu-K_α radiation (λ: 1.5438 Å) as the X-ray source. UV-visible spectra were recorded by Perkin-Elmer Lambda 35 UV-visible spectrometer. For this purpose, samples were prepared by sonication in double-distilled water for about 10 min and transferred into a quartz cuvette. FT-IR spectra of powder samples were recorded in a 1000 Perkin Elmer FT-IR spectrometer. Microscopy of the samples was carried out using FEI Tecnai T-20 200 kV transmission electron microscope (TEM). Atomic force microscopy (AFM) experiments were recorded using Digital Instrument Veeco Multimode AFM. Rotating disk

electrode experiments were conducted using Autolab RDE setup and Autolab potentiostate/galvanostate model PGSTAT 30. The rotation speed of RDE was varied in a wide range from 100 to 3000 rpm while sweeping the potential at 10 mV s^{-1} in ORR range. The reference electrodes used include saturated calomel (SCE) in the neutral electrolyte, Hg/HgO, 1 M KOH (MMO) in the alkaline electrolyte and a Pt wire pseudo reference electrode in the non-aqueous electrolyte. All potential values are converted into standard hydrogen electrode (SHE) scale and are presented. Charge-discharge cycling of Li-O_2 cells was carried out by using Bitrode battery cycling equipment in an air-conditioned room at 22 ± 1 ^{0}C.

RESULTS AND DISCUSSION

Physicochemical studies-Formation of RGO and Ag-RGO from graphite powder was examined by powder XRD studies. The patterns of graphite, GtO, GO, RGO and Ag-RGO are shown in Fig. 1. Graphite (Fig.1a curve i) is characterized by the strong (002) reflection at 26.5^0, corresponding to hexagonal graphitic structure. The inter-layer distance of (002) reflection obtained for graphite is 3.38 Å. This value is comparable with the reported values.[25] In the pattern of GtO, the (002) reflection is shifted to 10.3^0 (Fig.1a curve ii). This value corresponds to an inter-layer distance of 8.48 Å, indicating expansion of graphite due to the presence of oxygen containing functional groups on both sides of graphene sheets and also atomic scale roughness due to sp^3 bonding in carbon.[26] There is a shift in the (002) reflection of GO (Fig. 1a curve iii) indicating the conversion of GtO to GO. RGO is characterized by the low intensity, broad (002) reflection (Fig. 1a curve iv). It is known that the diffraction peaks become weak or even disappear when regular stacking of GO is disturbed.[27] The broad, weak (002) reflection is also attributed to small sheet size (≤ 1 μm) and a short domain order or turbostatic arrangement of RGO stacked sheets.[28] The XRD pattern of Ag-RGO (Fig. 1b) consists of a broad reflection at 24.2^0 corresponding to the (002) plane of RGO and strong reflections at 38.1, 44.3, 64.4 and 77.4^0, which are assigned to (111), (200), (220) and (311) planes, respectively, of face-centered cubic structure of Ag (JCPDS file 04-0783). Thus, XRD studies (Fig. 1) suggest the conversion

of graphite powder to RGO and Ag-RGO via formation of intermediates of GtO and GO. AFM data of RGO and Ag-RGO are presented in Fig. SI 1. The thickness values of RGO are about 2 and 5 nm, respectively, in bare RGO and Ag-RGO composite. Different values of thickness ranging from 0.35 to 1.0 nm are reported for single graphene layer. It is thus inferred that the RGO and Ag-RGO prepared in the present study consists of a few layers of graphene.[29]

UV-visible spectra of GO, RGO and Ag-RGO are presented in Fig. 2a. The 245 nm band of GO (Fig. 2a curve i) is a characteristic feature of π-π* transition of aromatic C-C bond and the shoulder at 307 nm is attributed to n-π* transition of C=O bond.[30] The spectrum of RGO (Fig. 2 curve ii) is characterized by 262 nm band, which is red shifted from 245 nm of GO. The absence of 307 nm shoulder indicates reduction of GO to RGO. In the spectrum of Ag-RGO (Fig. 2 curve iii), a new band at 410 nm appears which is attributed to electronic interaction of Ag nanoparticles with graphene sheets.[31] IR-spectra of GO and Ag-RGO are shown in Fig. 2b. The band at 3620 cm^{-1} present in the spectrum of GO (Fig. 2b curve i) is attributed to stretching of O-H bond on the GO surface (Table SI 1). The bands at 1709, 1584, 1222 and 1039 cm^{-1} are assigned to C=O, C=C, C-OH and C-O stretching vibrations, respectively. In the spectrum of Ag-RGO (Fig. 2b curve ii), the absorption bands at 3620 cm^{-1} (O-H bond) and 1709 cm^{-1} (C=O bond) are absent suggesting the reduction of GO to RGO.[32] XPS spectrum of Ag-RGO corresponding to 3d core level of Ag (Fig SI 2) consists of a doublet at 368.3 and 374.3 eV. The sepration of $3d_{5/2}$ and $3d_{3/2}$ by 6.0 eV indicates the metallic nature of Ag on RGO sheets.[33]

SEM images (Fig. 3a and b) indicate a layer-like morphology in both RGO and Ag-RGO samples. TEM images, particle size distribution and electron diffraction pattern of Ag-RGO sample are presented in Fig. 3c-f. The TEM images (Fig. 3c and d) reveal the presence of layers of RGO and nanoparticles of Ag distributed uniformly on them. Particle size distribution plot (Fig. 3e) suggests the presence of Ag particles in 2-7 nm range with an average size of 4.7 nm. The preparation of Ag-RGO involves simultaneous reduction of Ag^{+} ions and GO present in the reaction medium by ethylene glycol. It is interesting to note that Ag nanoparticles are anchored

uniformly over the sheets of RGO, instead of existing as seprate phase. It is thus inferred that Ag^+ ions are adsorbed on the surface of GO sheets, which possess interlayer separation of 8.48 Å. This is due to the presence of oxygen species on GO surface and their chemical interaction with Ag^+ ions. Subsequent to the addition of ethylene glycol, GO as well as the adsorbed Ag^+ ions undergo simultaneous reduction, thus, producing Ag anchored RGO layers. Electron diffraction pattern (Fig. 3f) indicates polycrystalline nature of Ag nanoparticles.

Electrochemical studies in KOH electrolyte- Cyclic voltammetry of GO and RGO coated GC electrodes indicated that reduction of O_2 did not take place in 1M KOH electrolytes. Voltammograms of Ag-RGO coated GC electrode were recorded in O_2 saturated as well as N_2 saturated KOH electrolyte (Fig. SI 3). When scanned from 0.24 V to -0.04 V, there was a reduction current peak at -0.06 V in O_2 saturated 1M KOH electrolyte. By repeating the experiment after saturating with N_2 gas, the reduction peak disappeared. Several repetitions were carried out by passing O_2 and N_2 gases alternately, and ensured that the reduction peak appearing at -0.06 V originated from O_2. Thus the current peak was attributed to the reduction of O_2(Reaction 1) catalyzed by Ag nanoparticles dispersed on RGO.

$$O_2 + 2H_2O + 4e^- \longrightarrow 4OH^- \quad (1)$$

The voltammograms of Ag-RGO were broad without sharp current peak corresponding to reaction (1). This was likely to be due to capacitance behaviour of RGO, which was due to adsorption of ions from the electrolyte. Experiments were repeated at several sweep rates (ν), and dependence of peak current density (i_p) on sweep rate was examined. A linearity of i_p versus $\nu^{1/2}$ plot indicated diffusion controlled reduction of ORR on Ag-RGO electrode.[34] Thus it was concluded that Ag nanoparticles dispersed on RGO catalysed ORR, but RGO and GC did not exhibit catalytic activity in the alkaline electrolyte.

Linear sweep voltammograms of Ag-RGO coated GC were recorded at a sweep rate of 10 mV s^{-1} with different speeds of RDE in 1M KOH solution saturated with O_2 (Fig. 4a). At all

speeds of RDE, current is negligibly small between 0.24 and -0.04 V. Reduction current starts increasing at 0.04 V and at it is nearly steady between -0.11 and -0.86 V. Current between 0.40 to -0.11 V is due to mixed control by both electron transfer and diffusion. The steady-state current is due to diffusion controlled ORR (Reaction 1). The diffusion–limited steady current density (i_L) is related to velocity of RDE (ω = 2πf, f being the frequency in revolution per second) by Levich equation.[34]

$$i_L = 0.62\, n\, F\, D^{2/3}\, \eta^{-1/6}\; c^o\; \omega^{1/2} \qquad (2)$$

where D is diffusion coefficient of dissolved O_2, η is kinematic viscosity of solution, c^o is concentration of O_2 in electrolyte and other symbols have their usual definitions. The data presented in Fig. 4a suggest that the limiting current is a steady value between -0.26 and -0.86 V at low rpm values of the RDE. A plot of i_L versus $\omega^{1/2}$ is presented in Fig. 4b. The plot is linear suggesting the validity of Eq. (2).

In the limiting current region, current density depends on the rate of diffusion of O_2 across the stagnant layer as described above. This condition prevails in the potential range from -0.11 to -0.86 V (Fig. 4a). However, at low current densities in the potential range 0.24 to -0.04 V, electron-transfer controls the rate of the ORR. In the intermediate range of potential (-0.04 to -0.16 V), the reaction is mixed control. In this region, Koutesky-Levich equation is valid.[34]

$$\frac{1}{i} = \frac{1}{nFkc^o} + \frac{1.61\,\eta^{1/6}}{nFc^oD^{2/3}}\frac{1}{\omega^{1/2}} \qquad (3)$$

where k is rate constant of reaction (1). A plot of i^{-1} versus $\omega^{-1/2}$ is expected to be linear. In Fig. 4c, i^{-1} versus $\omega^{-1/2}$ plots at different potentials in the range from -0.06 to -0.16 V are presented. The average value of D calculated from the slopes is 1.78 x 10^{-5} cm^2 s^{-1}, which agrees well with the value reported in the literature.[35] The values of k obtained from the intercepts (Fig. 4c) are in the range 6.1 to 3.1 cm^2 s^{-1}.

In the electron-transfer controlled region, current-potential data were measured potentiostatically while stirring 1 M KOH solution, which was saturated with O_2 gas. The data are presented as Tafel plot in Fig. 5. The slope of Tafel plot is 61.2 mV decade^{-1}, which indicates that the rate determining step involves a 2-electron transfer in the potential regime of fast mass transport.[36]

Electrochemical studies in K_2SO_4 electrolyte- Voltammograms of Ag-RGO coated GC electrode recorded in O_2 saturated as well as N_2 saturated 0.1 M K_2SO_4 electrolyte (Fig. SI 4) indicated the occurrence of ORR (Reaction 1) catalysed by Ag nanoparticles dispersed on RGO. A linearity of i_p vs. $\nu^{1/2}$ indicated diffusion controlled cyclic voltammetric reduction of ORR on Ag-RGO electrode. Thus it was concluded that Ag nanoparticles are active for ORR in 0.1M K_2SO_4 solution also. It was also observed that RGO and GC did not exhibit catalytic activity of ORR in 0.1 M K_2SO_4 electrolyte.

Linear sweep voltammograms of Ag-RGO coated GC electrode were recorded at sweep rate of 10 mV s^{-1} with different speeds in 0.1 M K_2SO_4 solution saturated with O_2. At all speeds of RDE, reduction current starts increasing at 0.14 V and it became nearly steady at -0.010 V. Current between 0.14 to -0.010 V is due to mixed control and the steady state current is due to diffusion controlled ORR (Reaction 1). Current density versus $\omega^{1/2}$ plot at-0.50 V is presented in Fig. 6b. The plot is linear suggesting the validity of Levich equation. Using the value of c^o for O_2 in 0.1 M K_2SO_4 solution (1.9 x 10^{-6} mol cm^{-3}), and ν (0.01), the value of D of O_2 (1.9 x 10^{-5} cm^2 s^{-1}). The number of electrons involved in oxygen reduction is calculated as 3.6.

In Fig. 6c, i^{-1} versus $\omega^{-1/2}$ plots at different potentials in the range from 0.04 to -0.06 V are presented. The average value of D calculated from the slopes is 1.95 x 10^{-5} cm^2 s^{-1}, which agrees well with the value reported.[37] The values of k obtained from the intercepts (Fig. 6b) are in the range 24.7 to 9.6 cm s^{-1}. In the electron-transfer controlled region, current-potential data were measured potentiostatically in stirred 0.1 M K_2SO_4 solution, which was saturated with O_2 gas.

The data are presented as Tafel plot in Fig. 7. The slope of Tafel plot is 151 mV decade^{-1}, indicating a complex reaction mechanism in neutral electrolyte. A Tafel slope of 120 mV decade^{-1} is expected if the rate determining step is 1-electron transfer process, such as the formation of superoxide (O_2^-) from O_2. As the Tafel slope is 151 mV decade^{-1}, it is inferred that adsorption process influences the kinetics of ORR in 0.1 M K_2SO_4 electrolyte.[38]

Electrochemical studies in non-aqueous electrolyte- Kinetics of ORR were studied using cyclic voltammetry and RDE in acetonitrile consisting of different salt by Laoire et al.[7] Although, a Li salt solution is required as the electrolyte for Li-air cell studies, such an electrolyte is found unsuitable for RDE studies employing a catalyst coated glassy carbon electrode. Formation of Li_2O and Li_2O_2 from the ORR deposit on the electrode surface leading to irreproducibility of experimental results. Therefore, TBAP dissolved in DMSO was used for CV and RDE studies in the present work. Cyclic voltammograms recorded at several sweep rates in 0.1 M TBAP-DMSO electrolyte at Ag-RGO coated GC electrode are shown in Fig. 8a. A cathodic current peak appears at -0.73 V in the forward sweep at 10 mV s^{-1}, which is attributed to the reduction of O_2 resulting in the formation of $TBAO_2$.[7]

$$TBA^+ + O_2 + e^- \longrightarrow TBAO_2 \qquad (4)$$

The voltammograms shown in Fig. 8 are similar to those reported by Laoire et al.,[7] except that another pair of minor current peaks as reported in[7] is absent in Fig. 8a. The second minor cathodic peak was attributed to further reduction of $TBAO_2$ to TBA_2O_2 (reaction 5).[7]

$$TBAO_2 + TBA^+ + e^- \longrightarrow TBA_2O_2 \qquad (5)$$

The absence of current peak due to the above step in Fig. 8a is attributed to difference in experimental conditions which include the nature of catalyst, solvent, etc., between the present work and Ref.[7] Thus, the cathodic current peak (P_c) in Fig. 8a is attributed to reduction of O_2 and the anodic peak (P_a) to the opposite reaction. As the anodic charge is less than the cathodic

charge, it is inferred that oxygen reaction is partially reversible. The cathodic peak current density (i_{pc}) is considered to follow Randles-Sevcik equation (Eq. 6).[34]

$$i_{pc} = \left(2.69\ x\ 10^5\right) n^{3/2}\ D^{1/2}\ \nu^{1/2}\ c^o \qquad (6)$$

where n is number of electrons, D is diffusion coefficient of O_2, v is sweep rate and c^o is concentration of O_2 in the electrolyte. A plot of i_{pc} versus $\nu^{1/2}$ is a straight line (Fig. 8b) indicating the ORR is controlled by diffusion of O_2. Similar observation is made for the anodic peak current density (i_{pa}) also from i_{pa} versus $\nu^{1/2}$ data (Fig. 8b). The two plots (Fig. 8b) have two different slopes due to differences in kinetics of ORR and OER.

Linear sweep voltammograms recorded in O_2 saturated 0.1 M TBAP-DMSO solution at several rotation speeds of RDE are presented in Fig. 9a. Similar to the data obtained in aqueous electrolytes discussed above, the voltammograms (Fig. 9a) are characterized by electron-transfer controlled regime at low potentials, diffusion-controlled regime with limiting current at high potentials and a mixed regime in between. The low potential data were plotted as Tafel plot (Fig. SI 5) and slope of 53 mV decade^{-1} was obtained for the data recorded at 200 rpm. Similar values of slopes were obtained at higher rotation rates also. This value is close to 60 mV decade^{-1} expected for a 2-electron transfer process. It is thus inferred that the reduction of O_2 in non-aqueous electrolytes under electron-transfer controlled conditions occurs as 2-electon transfer process leading to the formation of O^{2-}. The diffusion controlled RDE data were analysed similar to the aqueous data and the values of D and n obtained are 1.62 x 10^{-6} cm^2 s^{-1} and 0.7, respectively. The value of n close to unity indicates the formation of superoxide (O_2^-) in the non-aqueous electrolyte under diffusion-limited conditions.

Li-O_2 cell study- The electrochemical properties of O_2 electrode of Li-O_2 cells in non-aqueous electrolytes depend on several factors including the properties of carbon, catalyst, nature of the current collector, method of electrodes fabrication and nature of the electrolyte. In the

present work, 1.0 M $LiPF_6$ dissolved in DMSO is used as the electrolyte and porous Toray carbon paper is used as the current collecting substrate. On one side of the carbon paper, a diffusion-layer made of high surface area (1500 cm^2 g^{-1}) carbon powder with micropores of diameter less than 2 nm was coated at a loading level of 185 mg cm^{-2}.[24] This side was exposed to O_2 gas. The other side of the carbon paper, which was exposed to the electrolyte, was coated with the catalyst. Several Li-O_2(Ag-RGO) cells were assembled and subjected to charge-discharge cycling with different currents. A few Li-O_2(RGO) cells without Ag catalyst were also assembled for comparison studies. Charge-discharge curves of Li-O_2(Ag-RGO) cells are presented in Fig. 10a for three different currents. The discharge capacity decreases with an increase in current as expected. At 0.2 mA cm^{-2}, the discharge plateau appears at about 2.50 V and the charge plateau at about 4.20 V. Thus, the difference in charge-discharge plateaus is about 1.70 V, which is a high value. For high reversible battery systems, the expected difference in charge-discharge plateaus is expected of the order of a few tens of mV. A large voltage gap is an inherent problem associated with Li-O_2 cells, which is observed, is several reports.[39-41] With an increase in current density, there is an increase in voltage gap. The discharge capacity values obtained are 11950 (11.29), 9340 (5), and 2780 mAh g^{-1} (2.47 mAh cm^{-2}), respectively, when discharged at 0.2, 0.5 and 0.8 mA cm^{-2}. It is interesting to note that the discharge capacity of 11950 mAh g^{-1} (11.29 mAh cm^{-2}) obtained at 0.2 mA cm^{-2} is an extremely high value. A wide range of discharge capacity values are reported in the literature. For instance, discharge capacity of 1400 mAh g^{-1} with cobalt phthalocyanine catalyst,[4] 1000 mAh g^{-1} with electrolytic MnO_2,[42] 3000 mAh g^{-1} with α-MnO_2,[43] 2700 mAh g^{-1} with Fe_2O_3,[44] 225 mAh g^{-1} with Pd-MnO_2,[45] 4750 mAh g^{-1} with MnO_2 catalyst,[46] 8706 mAh g^{-1} with graphene,[47] and 15,000 mAh g^{-1} with graphene catalyst[7] are reported for Li-O_2 cells. A comparison of discharge capacity obtained in the present study with the values reported in the literature could be inconclusive because there is no uniformity in experimental conditions such as cell configurations, current collectors,

electrodes fabrication, nature of the catalyst and its loading level, electrolytes, current densities used for charge-discharge cycling, etc.

The charge-discharge reactions occurring at the electrodes are as follows.

At the negative electrode:

$$Li^+ + e^- \underset{\text{discharge}}{\overset{\text{charge}}{\rightleftharpoons}} Li \qquad (7)$$

It is known that the reduction of O_2 in Li^+ ion containing non-aqueous electrolytes results in the formation of Li_2O_2 and Li_2O as stable products during the discharge of Li-O_2 cell. Laoire et al.,[7] proposed the following mechanism for oxygen electrode reactions:

$$O_2 + Li^+ + e^- \underset{\text{charge}}{\overset{\text{discharge}}{\rightleftharpoons}} LiO_2 \qquad (8)$$

$$LiO_2 + Li^+ + e^- \underset{\text{charge}}{\overset{\text{discharge}}{\rightleftharpoons}} Li_2O_2 \qquad (9)$$

$$Li_2O_2 + 2Li^+ + 2e^- \underset{\text{charge}}{\overset{\text{discharge}}{\rightleftharpoons}} 2Li_2O \qquad (10)$$

Single-electron transfer reduction of O_2 producing superoxide (O_2^-) in non-aqueous electrolytes (reaction 8) is reported.[7] Lithium superoxide undergoes another single-electron transfer reduction (reaction 9) forming lithium peroxide, which further undergoes two electron transfer reduction (reaction 10) forming the final reduction product, Li_2O. It is also reported that the reaction product is Li_2CO_3 in carbonate-based electrolyte.[48] It is also believed that the reaction intermediate formed during oxygen reduction, namely, O_2^- is reactive towards most of the solvents used for the electrolyte, which may lead to the formation of Li_2CO_3.[49] Li_2CO_3 cannot be oxidized back to O_2, thus affecting rechargeability and cycle-life of Li-O_2 cells. Alternate non-reactive solvents such as DMSO are suggested.[49] The electrolyte used in the present study is 1.0 M $LiPF_6$ dissolved in DMSO. Lithium oxides are expected to be the major reaction products of oxygen reduction in the non-carbonate based electrolytes.[50, 51] In the present study

also, Li_2O_2 and Li_2O are identified as the major products of O_2 reduction during the discharge of Li-O_2(Ag-RGO) cells, as discussed later. During the charging process, Li_2O_2 and Li_2O are converted to O_2 following the reverse steps of reactions 10, 9 and 8 in sequence.

Mechanistically, the adsorption of O_2 on the catalyst surface is expected to be the primary step of ORR. It is expected that the Ag nanoparticles anchored to RGO possess large surface defects facilitating adsorption O_2. The adsorbed O_2, thus, undergoes electron-transfer in the presence of Li^+ ions producing LiO_2, Li_2O_2 and Li_2O (reactions 8-10) during discharge of Li-O_2(Ag-RGO) cells. The reverse reactions occur resulting in OER during the charging process.

Li-O_2(Ag-RGO) cells were tested for cycling stability at a current density of 0.8 mA cm^{-2} over 30 cycles (Fig. 10b). Initially, about 2800 mAh g^{-1} (2.47 mAh cm^{-2}) is obtained. There is a rapid decrease in capacity to about 937 mAh g^{-1} (0.82 mAh cm^{-2}) at the 4^{th} cycle. This is followed by a gradual decrease in capacity. About 586 mAh g^{-1} (0.51 mAh cm^{-2}) is obtained at the 30^{th} cycle. When Li-O_2(RGO) cells were cycled, the discharge capacity decreased rapidly in about 5-10 cycles and the cells could not be cycled thereafter. These results confirm the catalytic activity of Ag-RGO for oxygen electrode reaction in non-aqueous rechargeable Li-O_2 cells. Thus, Ag-RGO is a promising catalyst for rechargeable Li-O_2 cells.

In order to identify the reaction products of O_2 reduction on Ag-RGO in DMSO electrolyte, a few Li-O_2(Ag-RGO) cells were assembled, subjected to five charge-discharge cycles and the cycling was terminated after the cells were discharged. The cells were dissembled, washed with acetone and XRD patterns of the oxygen electrodes were recorded (Fig. 11). The catalyst layers of a few used electrodes were scraped out of the carbon paper substrate and examined under TEM (Fig. SI6). The Ag nanoparticles are clearly observed on RGO of the used electrodes. There is an increase in particle size in comparison with fresh Ag-RGO (Fig. 3d). This may be due to mechanical stresses involved in the preparation of the electrodes and also in scraping of coating layers. The XRD patterns (Fig. 11) recorded for all electrodes were similar,

thus, ensuring the reproducibility of the results. The (002) reflection of carbon is present at 26.4^0. This is the most intense peak of the XRD pattern (Fig. 11) because of the presence of porous carbon paper current collector, diffusion layer made of carbon powder and also RGO present in Ag-RGO catalyst. The reflections corresponding to (111), (200), (220) and (311) planes of face-centered cubic crystal of Ag appear at 38.1, 44.3, 64.4 and 77.4^0, respectively (Fig. 11). These reflections remain the same as those of the as prepared Ag-RGO catalyst (Fig. 1b). As there are no changes noticed in the crystal structure of Ag after repeated charge-discharge cycling, the stability of the catalyst is ensured. In addition to the reflections of carbon and Ag, there are a few more peaks or shoulders present in the cycled electrode. The reflection at 18.2^0 is attributed to the PTFE binder present in the electrode, the peak at 21.5, 32.1, 34.8 and 48.8^0 are due to Li_2O_2, and a weak peak at 54.4^0 is due to Li_2O. Low intensity peaks present at 31.1 and 33.7^0 are attributed to LiOH probably formed by hydrolysis of oxides of Li during handling of the electrodes in ambient atmosphere. Thus, Li_2O_2 and Li_2O are inferred as the products of O_2 reduction in the present study.

CONCLUSIONS

Silver nanoparticles anchored reduced graphene oxide (Ag-RGO) was prepared by simultaneous reduction of graphene oxide and Ag^+ ions in an aqueous medium by ethylene glycol as the reducing agent. Ag particles of average size of 4.7 nm were uniformly distributed on the RGO sheets. Ag-RGO possesses catalytic activity towards ORR in both aqueous and non-aqueous electrolytes. Li-O_2 cells were assembled using Ag-RGO as the catalyst for rechargeable oxygen electrode.The cells were subjected to charge-discharge cycling at several current densities. A discharge capacity of 11,950 mAh g^{-1} (11.29 mAh cm^{-2}) was obtained initially at low a current density. Although there was a decrease in capacity on repeated discharge-charge cycling initially, a stable capacity was observed for about 30 cycles. The results indicated that Ag-RGO was a promising catalyst for rechargeable Li-O_2 cells.

References:-

[1] E. Yeager, *J. Mol. Catal.,* 1986, **38**, 5-25.

[2] M. K. Debe, *Nature,* 2012, **486**, 43-51.

[3] J-S Lee, S. T. Kim, R. Cao, N-S Choi, M. Liu, K. T. Lee, and J. Chao, *Adv. Energy Mater*., 2011, **1**, 34-50

[4] K. M. Abraham, and Z. Jiang, *J. Electrochem. Soc*., 1996, **143**, 1-5.

[5] G. Girishkumar, B. McCloskey, A. C. Luntz, S. Swanson, and W. Wilcke, *J. Phys. Chem. Lett.,* 2010, **1**, 2193-2203.

[6] A. Damjanovic, M. A. Genshaw, and J. O. M. Bockris, *J. Electroanal. Chem.,* 1967, **15**, 173- 180.

[7] C. O. Laoire, S. Mukerjee, and K. M. Abraham, *J. Phys. Chem. C*., 2009, **113**, 20127-20137.

[8] V. Di. Noto, E. Negro, S. Polizzi, F. Agresti, and G. A. Giffin, *ChemSusChem,* 2012, **5**, 2451– 2459.

[9] V. Di. Noto, E. Negro, K. Vezzu, L. Toniolo, and G. Pace, *Electrochim. Acta*, 2011, **57**, 257–269.

[10] V. Di. Noto, and E. Negro, *J. Power Sources*, 2010, **195**, 638-648.

[11] V. Di. Noto, and E. Negro, *Electrochim. Acta*, 2010, **55**, 7564–7574.

[12] P. Singh, and D. A. Buttry, *J. Phys. Chem. C,* 2012, **116**, 10656-10663.

[13] A. K. Geim, and K. S. Novoselov, *Nature Mater.,* 2007, **6**, 183-191.

[14] S. Bose, T. Kuila, A. K. Mishra, R. Rajasekar, N. H. Kim, and J. H. Lee, *J. Mater. Chem.,* 2012, **22**, 767-784.

[15] M. Liang, and L. Zhi, *J. Mater. Chem.,* 2009, **19**, 5871–5878.

[16] E. Antolini, *Appl. Catal. B: Env.,* 2012, **123– 124**, 52– 68.

[17] E. J. Lim, S. M. Choi, M. H. Seo, Y. Kim, S. Lee, and W. B. Kim, *Electrochem. Commun*., 2013, **28**, 100–103.

[18] D. J. Davis, A-R O. Raji, T. N. Lambert, J. A. Vigil, L. Li, K. Nan, and J. M. Tour, *Electroanal.,* 2014, **26**, 164 – 170.

[19] L. Lu, J. Liu, Y. Hu, Y. Zhang, and W. Chen, *Adv. Mater*., 2013, **25**, 1270-1274.

[20] W. S. Hummers Jr. and R. E. Offeman, *J. Am. Chem. Soc.,* 1958, **80**, 1339.

[21] S. Kumar, S. Ghosh, N. Munichandraiah, and H. N. Vasan, *Nanotechnology*, 2013, **24**, 235101 (9p).

[22] M. Eswaran, N. Munichandraiah, and L. G. Scanlon, *Electrochem. Solid-State Lett.,* 2010, **13**, A121-A124.

[23] C. Selvaraj, N. Munichandraiah, and L. G. Scanlon, *J. Porphyrins Phthalocyanines,* 2012, **16**, 255-259.

[24] S. Kumar, C. Selvaraj, N. Munichandraiah, and L. G. Scanlon, *RSC Adv.,* 2013, **3**, 21706-21714.

[25] J. Yang, C. Zhang, L. Sun, N. Zhao, and X. Cheng, *Mater. Chem. Phys.,* 2011, **129**, 270-274.

[26] J. Shen, Y. Hu, M. Shi, X. Lu, C. Qin, and C. Li, *Chem. Mater.,* 2009, **21**, 3514-3520.

[27] C. Xu, X. Wang, L. Yang, and Y. Wu, *J. Solid State Chem*., 2009, **182**, 2486-2490.

[28] S. Dubin, S. Gilje, K. Wang, V.C. Tung, K. Cha, A.S. Hall, J. Farrar, R. Varshneya and Y. Yang, and R. B. Kaner, *ACS Nano,* 2010, **4**, 3845-3852.

[29] P. Nemes-Incze, Z. Osvath, K. Kamaras, and L. P. Biro, *Carbon*, 2008, **46**, 1435-1442.

[30] Z. Sun, Z. Yan, J. Yao, E. Beitler, Y. Zhu, and J. M. Tour, *Nature,* 2010, **468**, 549-552.

[31] T. A. Pham, B. C. Choi, K. T. Lim, and Y. T. Jeong, *Appl. Surf. Sci.*, 2011, **257**, 3350–3357.

[32] K Bramhaiah, and N S John, *Adv. Nat. Sci.: Nanosci. Nanotechnol*., 2012, **3**, 045002 (6p).

[33] P. Prieto, V. Nistor, K. Nouneh, M. Oyama, M. Abd-Lefdil, and R. Diaz, *App. Surf. Sci.*, 2012, **258**, 8807– 8813

[34] A. J. Bard, and L. R. Faulkner, *Electrochemical Methods: Fundamental and Application*, John Wiley and Sons, 1980.

[35] X. Zhou, Z. Yang, H. Nie, Z. Yao, L. Zhang, and S. Huang, *J Power Sources,* 2011, **196**, 9970–9974.

[36] Zhang. J. (Ed), *PEM Fuel Cell Electrocatalyst and Catalyst Layers: Fundamental and Application*, 2008, ISBN: 978-1-84800-935-6.

[37] I. Roche, and K. Scott, *J. Appl. Electrochem.*, 2009, **39**, 197–204.

[38] N. M. Markovic, H. A. Gasteiger, and P. N. Ross, *J. Phys. Chem*., 1996, **100**, 6715-6721.

[39] Y. Li, J. Wang, X. Li, D. Geng, R. Li, and X. Sun, *Chem. Commun.,* 2011, **47**, 9438–9440.

[40] Y-C Lu, H. A. Gasteiger, M. C. Parent, V. Chiloyan, and Y. Shao-Horn, *Electrochem.*

Solid State Lett., 2010, **13**, A69-A72.

[41] N. Imanishi, and O. Yamamoto, *Mater. Today*, 2014, **17**, 24-30.

[42] T. Ogasawara, A. Debart, M. Holzapfel, P. Novak, and P. G. Bruce, *J. Am. Chem. Soc.*, 2006, **128**, 1390-1393.

[43] A. Debart, A. J. Paterson, J. Bao, and P. G. Bruce, *Angew, Chem. Int. Ed.*, 2008, **47**, 4521-4524.

[44] A. Debart, J. Bao, G. Armstrong, and P. G. Bruce, *J. Power Sources*, 2007, **174**, 1177-1182.

[45] A. K. Thapa, K. Saimen, and T. Ishihara, *Electrochem. Solid-State Lett.*, 2010, **13**, A165-A167.

[46] H. Cheng, and K. Scott, *J. Power Sources*, 2010, **195**, 1370-1374.

[47] Y. Li, J. Wang, X. Li, D. Geng, R. Li, and X. Sun, *Chem. Comm.*, 2011, **47**, 9438-9440.

[48] S. A. Freunberge, Y. Chen, Z. Pneg, J. M. Griffin, L. J. Hard-wick, F. Bard, P. Novak, and P. G. Bruce, *J. Am. Chem. Soc*., 2011, **133**, 8040-8047.

[49] D. Xu, Z. Wang, J. Xu, L. Zhang and X. Zhang, *Chem. Comm*., 2012, **48**, 6948 – 6950.

[50] S. A. Freunberger, Y. Chen, N. E. Drewett, L. J. Hardwick, F. Barde, and P. G. Bruce, *Angew. Chem. Int. Ed*., 2011, **50**, 8609-8613.

[51] D. Sharon, V. Etacheri, A. Garsuch, M. Afri, A. A. Frimer, and D. Aurbach, *J. Phys. Chem. Lett*., 2013, **4**, 127-131.

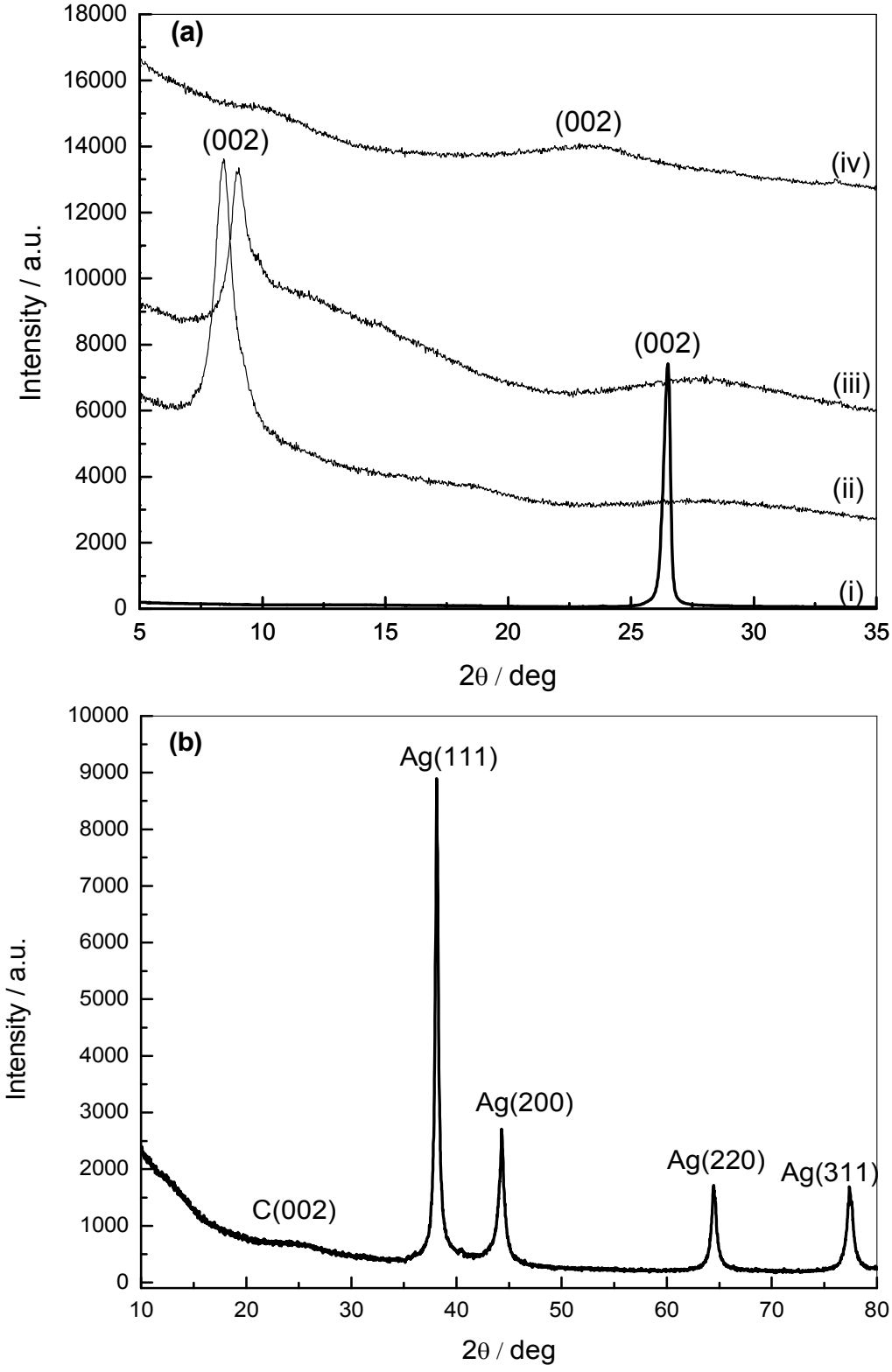

Fig. 1. (a) Powder XRD pattern of graphite (i), graphite oxide (GtO) (ii), graphene oxide (GO) (iii) and reduced grapheme oxide (RGO) (iv), and (b) powder XRD pattern of Ag-RGO.

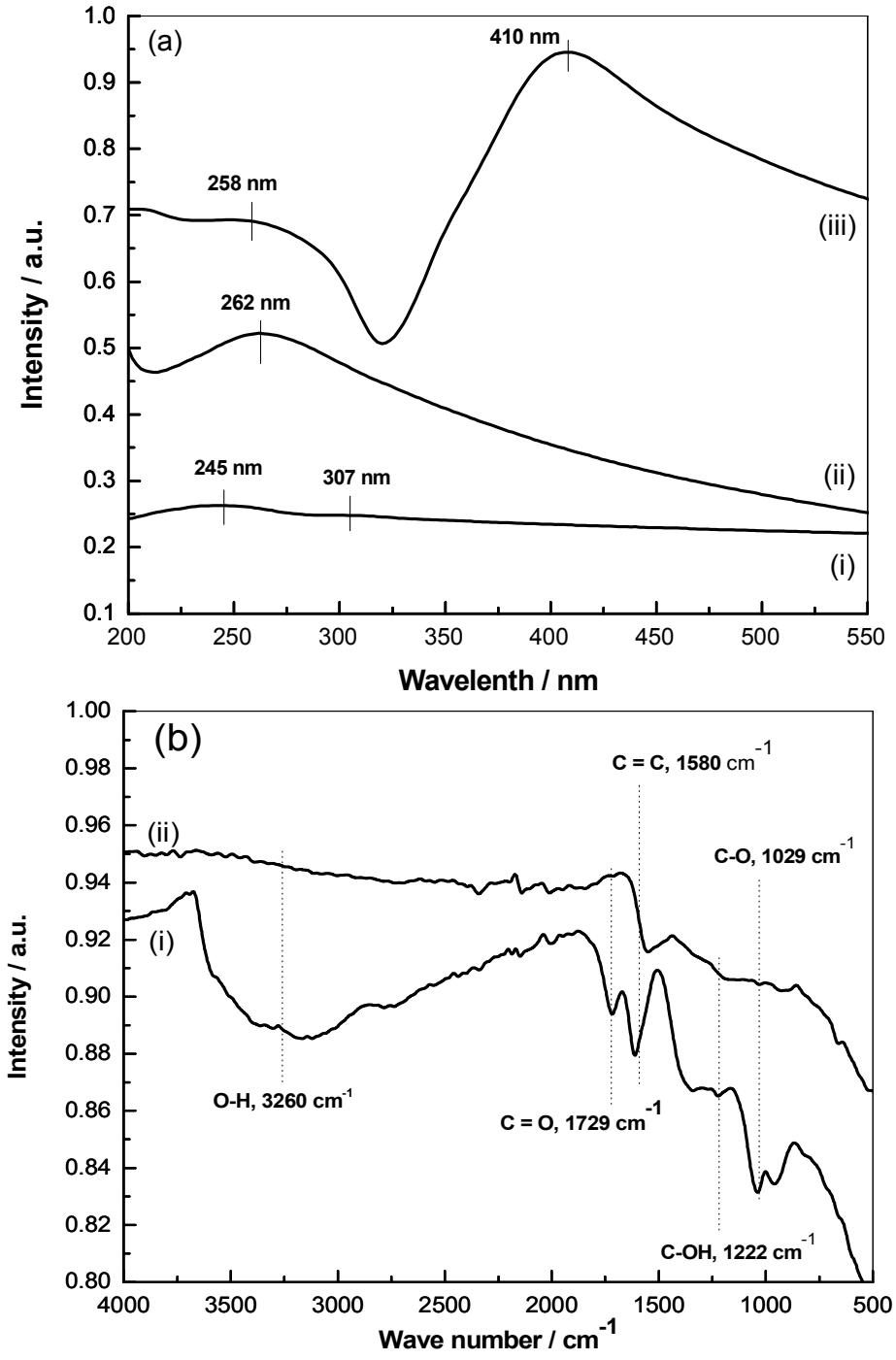

Fig.2. (a) UV spectra of graphene oxide (i), RGO (ii), and Ag-RGO (iii), (b) IR spectra of graphene oxide (i) and Ag-RGO (ii).

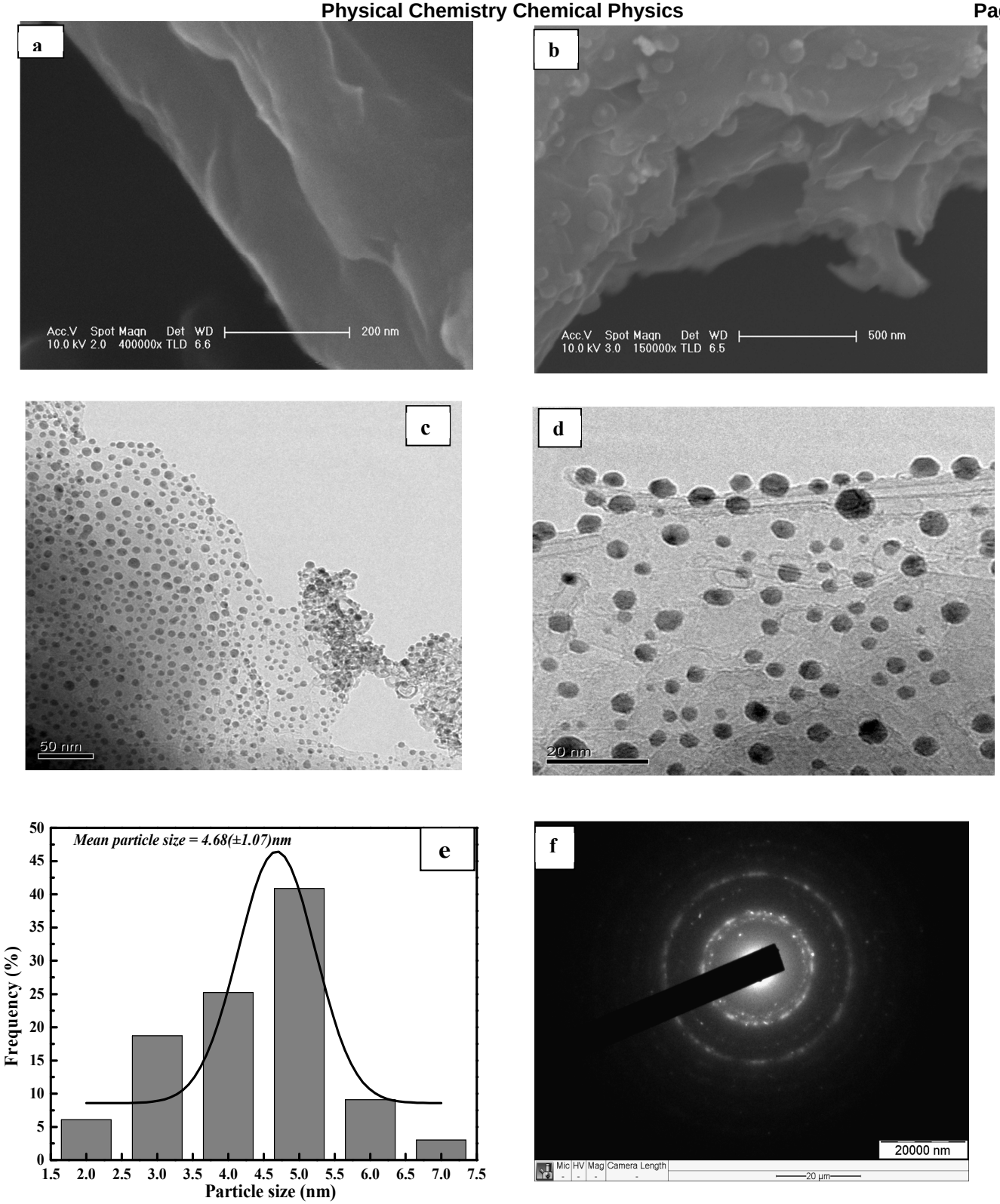

Fig. 3. SEM images of RGO (a) and Ag-RGO (b), TEM images of Ag-RGO in different magnifications (c, d), particle size distribution of Ag-RGO (e) and diffraction pattern of Ag-RGO (f).

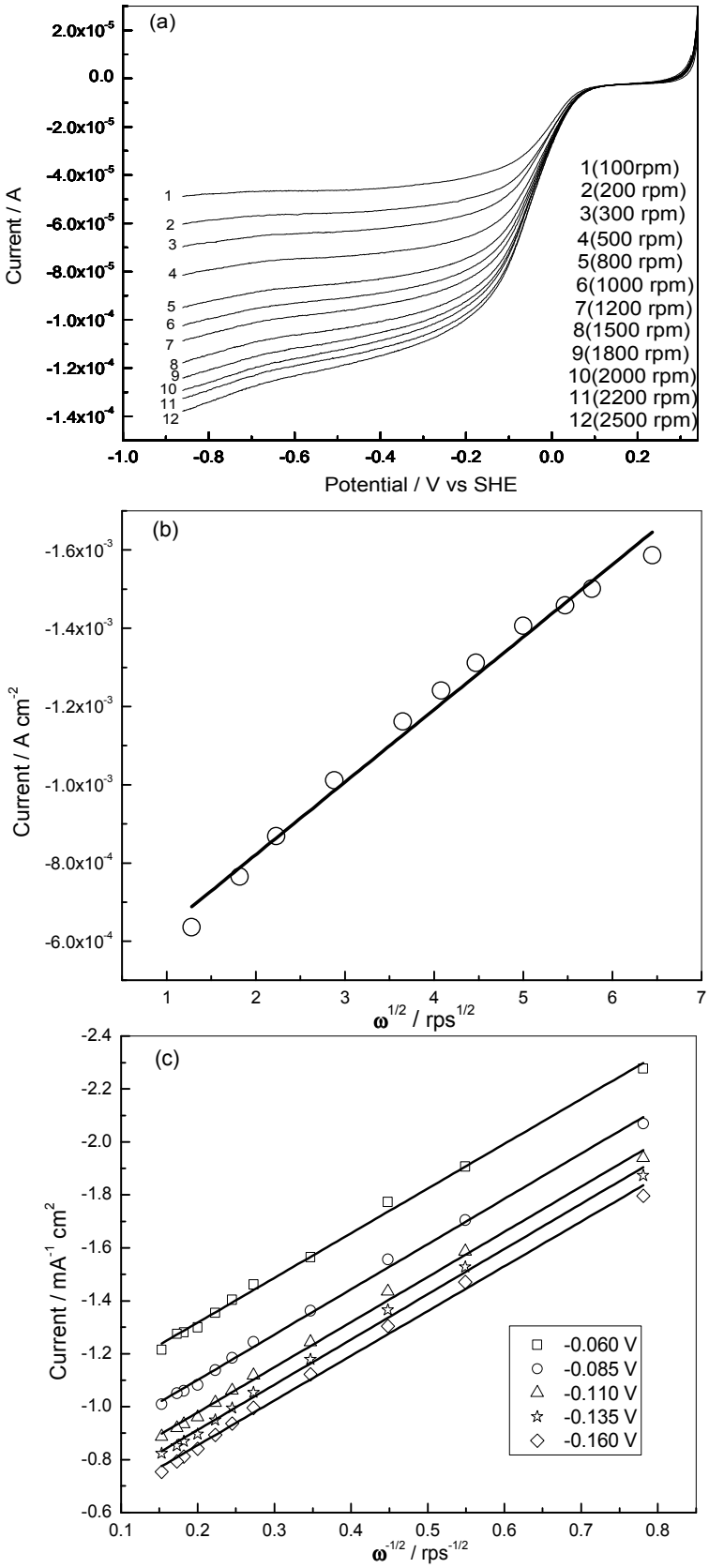

Fig. 4. (a) Linear sweep voltammetry for ORR at 10 mVs^{-1} after saturation with O_2 gas in 1M KOH in rotation speed range from 100 to 2500 rpm, (b) Levich plot, and (c) Koutecky-Levich plot.

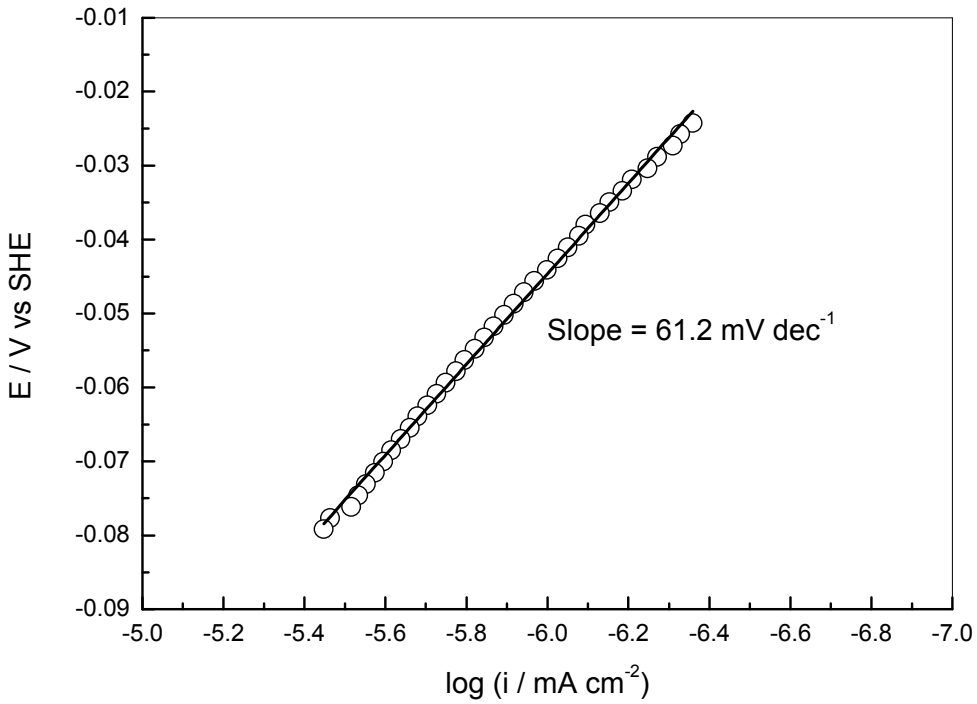

Fig. 5. Tafel plot of ORR in 1M KOH.

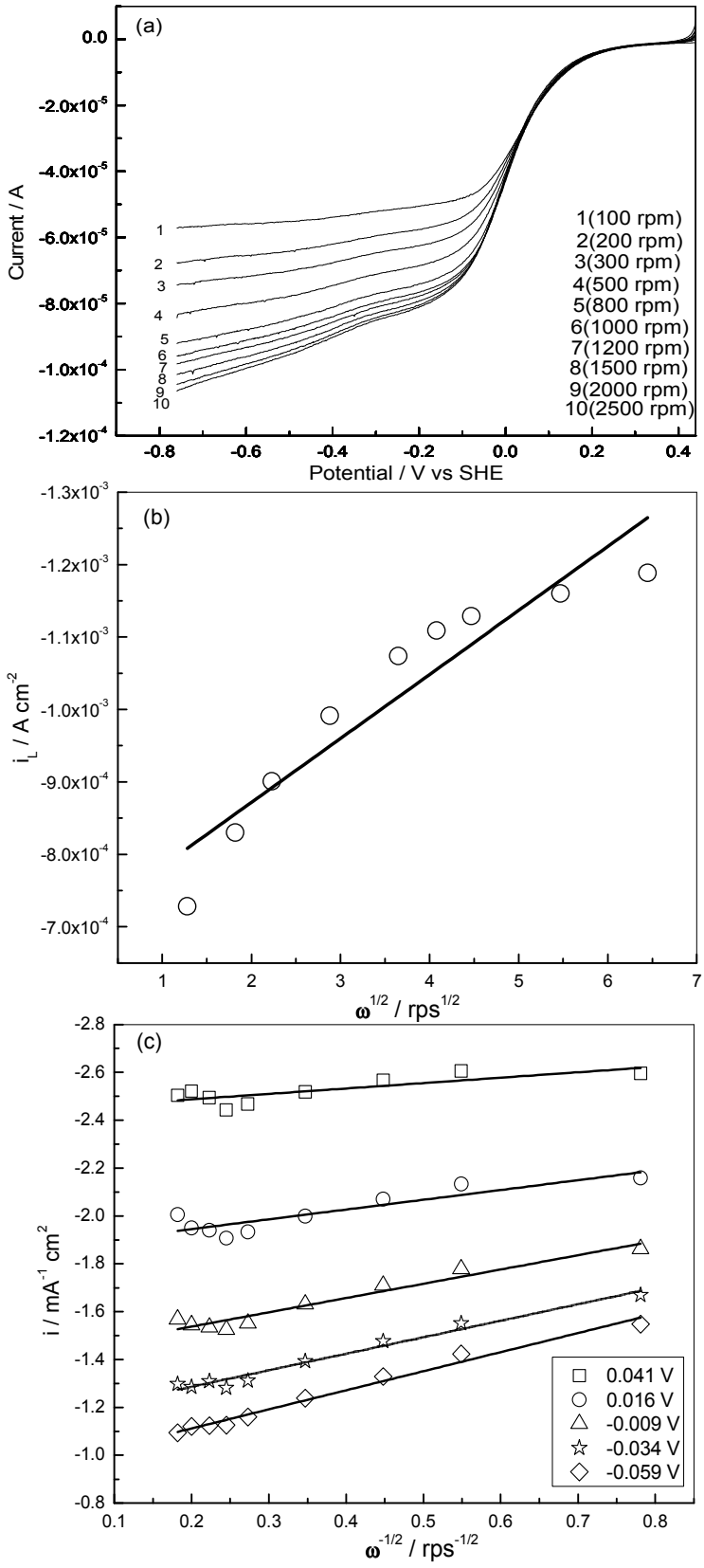

Fig. 6. (a) Linear sweep voltammetry for ORR at 10 mVs^{-1} scan rate after saturation with O_2 gas in 0.1M K_2SO_4 in rotation speed range from 100 to 2500 rpm, (b) Levich plot, (c) Koutecky-Levich plot.

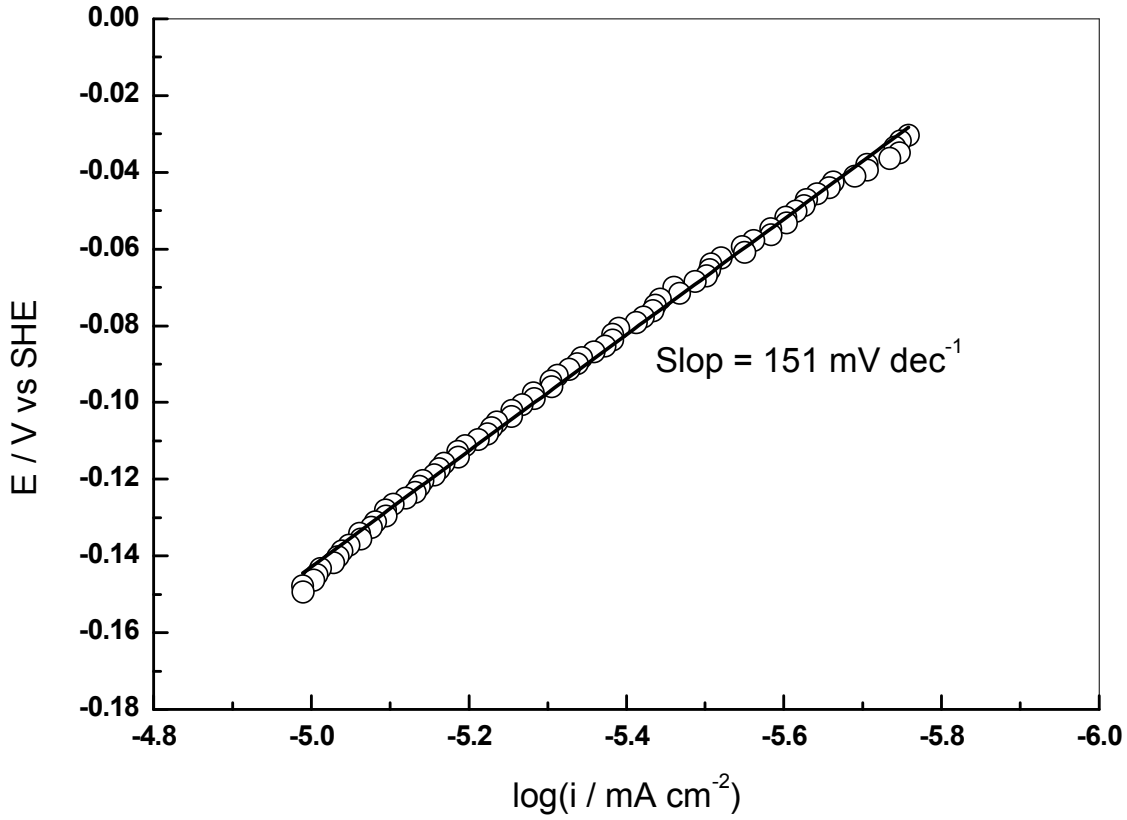

Fig. 7. Tafel plot of ORR in 0.1 M K_2SO_4.

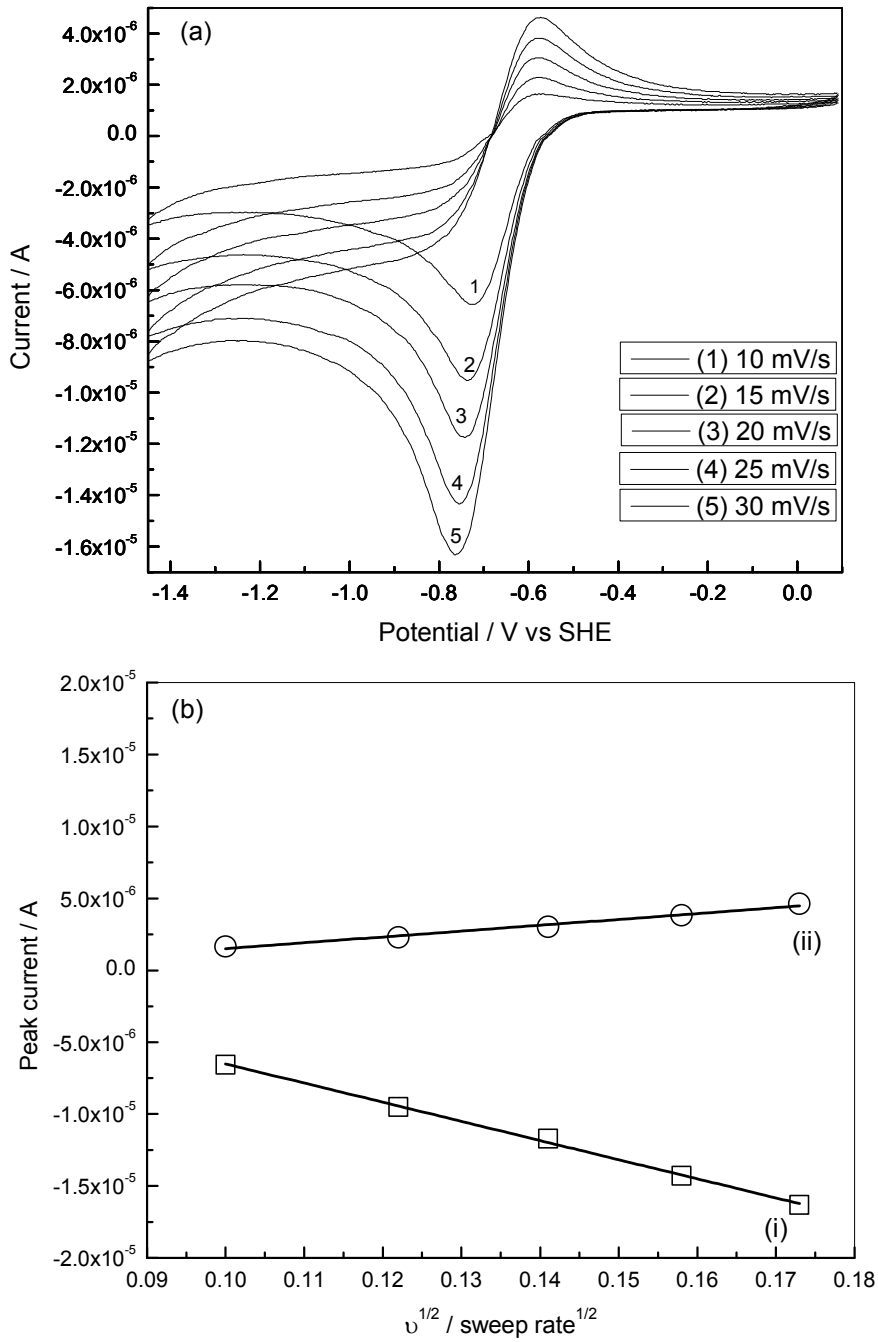

Fig. 8. (a) Cyclic voltammetry for ORR activity at different scan rates and (b) plot between peaks current versus (sweep rate)$^{1/2}$ in 0.1M TBAP-DMSO; for (i) cathodic and (ii) anodic peak.

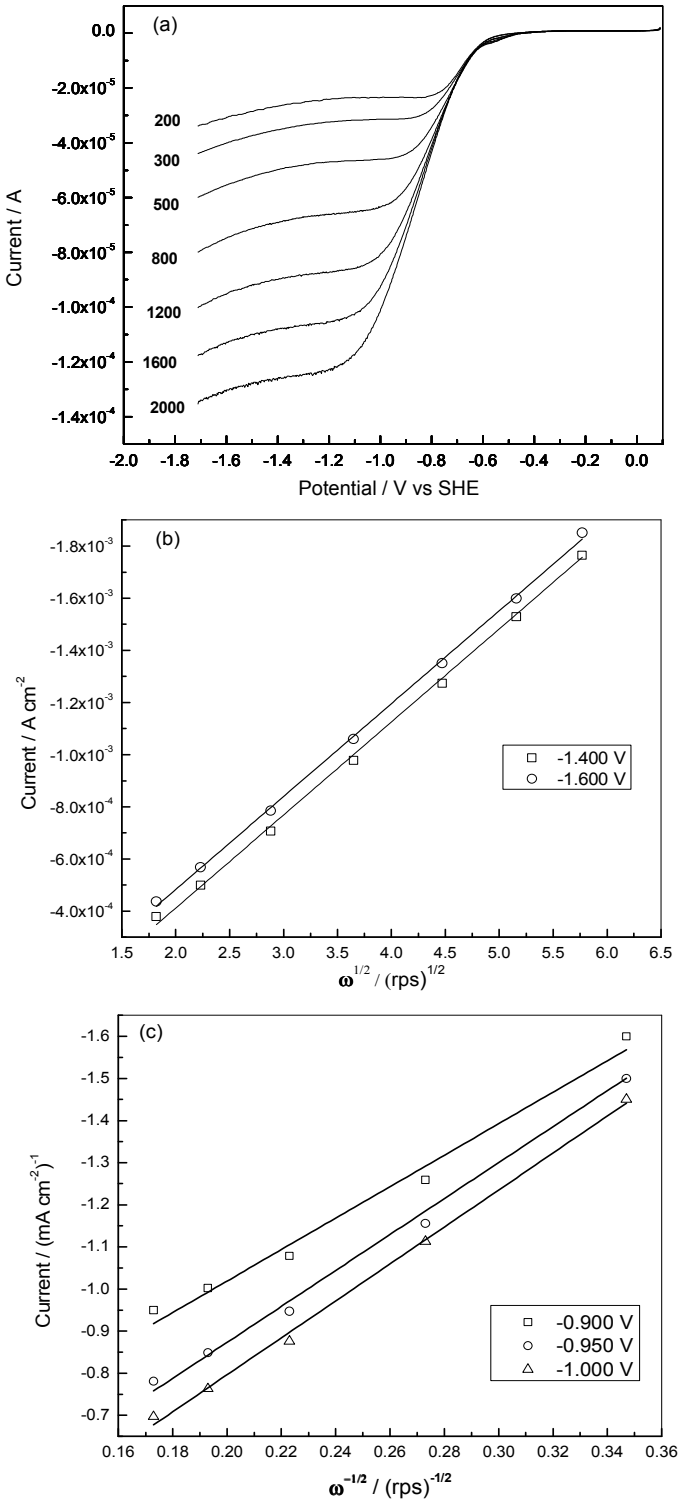

Fig. 9. (a) Linear sweep voltammetry for ORR at 10 mV s^{-1} scan rate with different speed of rotationin 0.1M TBAP-DMSO,(b) Levich plot, and (c) Koutecky-Levich plot.

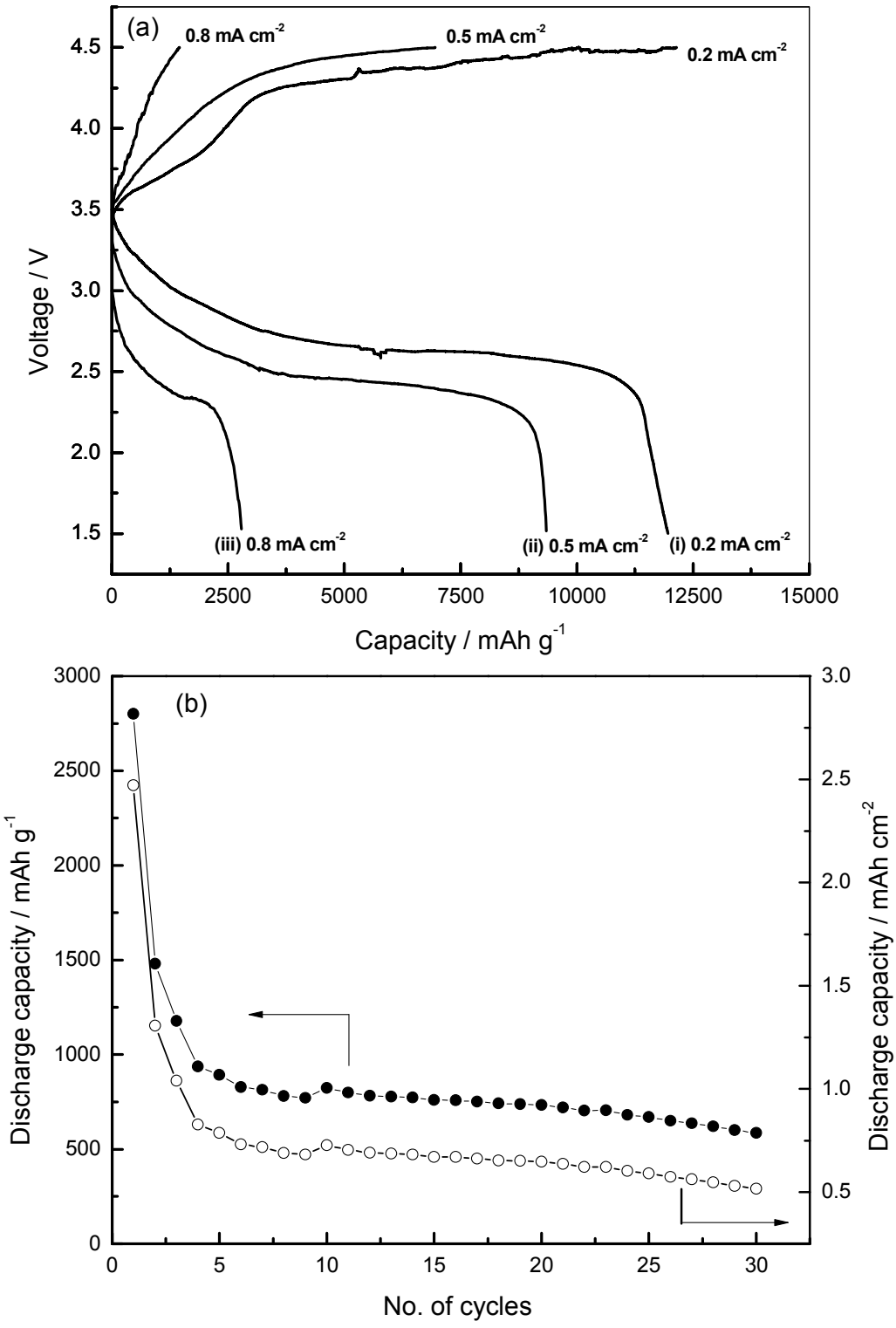

Fig. 10. (a) Comparison of discharge capacity of first cycle at different current densities and (b) cycle life test at current density 0.8mA cm^{-2}.

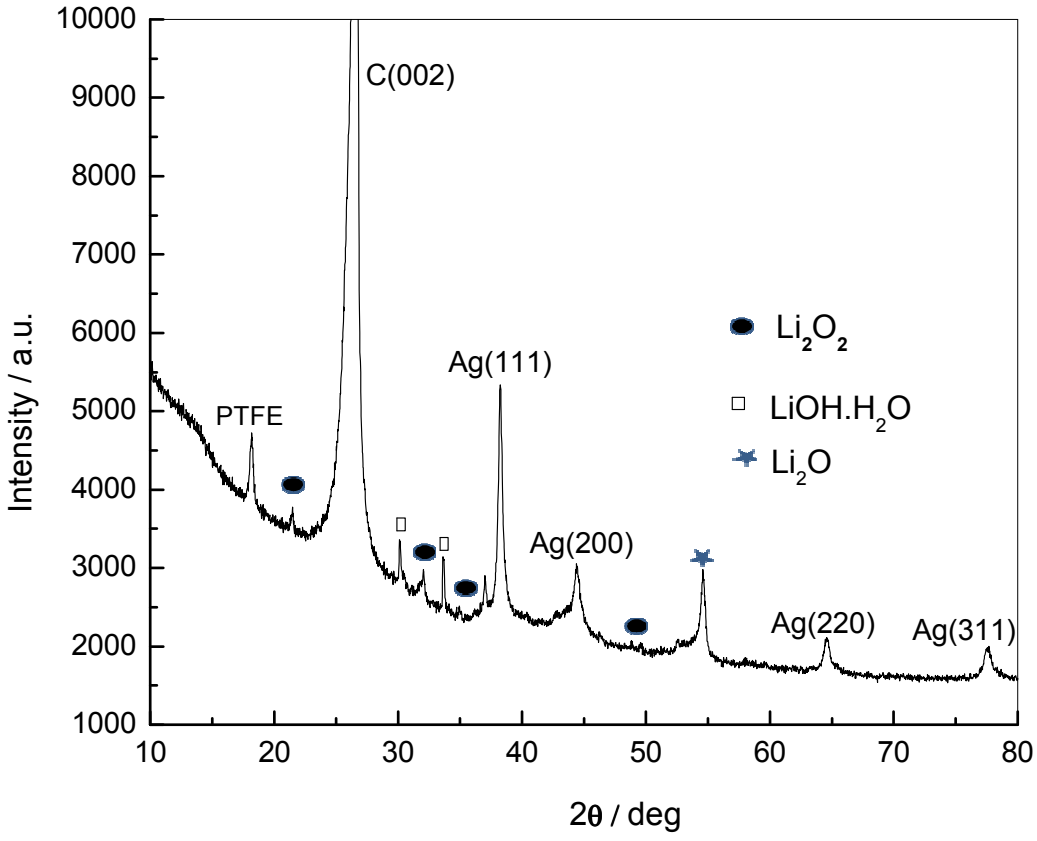

Fig.11. XRD pattern of oxygen electrode of Li-O_2(Ag-RGO) cell after subjecting to five charge-discharge cycles.